A New WENO Weak Galerkin Finite Element Method for Time Dependent Hyperbolic Equations

Lin Mu[1], Zheng Chen[2]

Abstract

In this paper, we develop a new WENO weak Galerkin finite element scheme for solving the time dependent hyperbolic equations. The upwind-type stabilizer is imposed to enforce the flux direction in the scheme. For the linear convection equations, we analyze the L^2-stability and error estimate for L^2-norm. We also investigate a simple limiter using weighted essentially non-oscillatory (WENO) methodology for obtaining a robust procedure to achieve high order accuracy and capture the sharp, non-oscillatory shock transitions. The approach applies for linear convection equations and Burgers equations. Finally, numerical examples are presented for validating the theoretical conclusions.

Keywords: Hyperbolic equations; weak Galerkin; finite element methods; upwind scheme; WENO limiter; Burgers equations.

1. Introduction

In this paper, we consider the following one-dimensional hyperbolic equations:

$$\frac{\partial u}{\partial t} + \beta \frac{\partial u}{\partial x} = 0, \quad (x,t) \in I \times J \tag{1}$$

$$u = 0, \quad x \in \Gamma^-, \tag{2}$$

with initial condition $u(x,0) = g(x)$. β is assumed to be a nonzero constant. Here $J = (0,T]$, $T \leq \infty$, and the homogeneous inflow boundary Γ^- condition is assumed for simplicity. We also denote the other boundary $\Gamma^+ := \partial I \backslash \Gamma^-$. In this paper, we assume I is a one dimensional domain.

The hyperbolic equations have broad applications in science and engineering, including fluid mechanics, aerodynamics, and many other areas. In many cases, the hyperbolic equations may have discontinuous solutions when the boundary or initial data is discontinuous. It is still a challenge to develop numerical methods for resolving discontinuities without significant spurious oscillations. The classical Burgers equation, which is in the class of nonlinear hyperbolic equations, has been a center of interest for researchers studying various physical phenomena such as theory of shock waves, fluid dynamics, turbulent flow and gas dynamics. Numerical solution of Burgers' equation is a natural and the first step towards developing methods for the computation of complex flows.

Email addresses: linmu@uga.edu (Lin Mu), zchen2@umassd.edu (Zheng Chen)
[1]Department of Mathematics, University of Georgia, Athens, GA 30602
[2]Department of Mathematics, University of Massachusetts, Dartmouth, MA, 02747

Various numerical methods have been proposed in the past for hyperbolic equations, including finite difference, finite volume, finite element, boundary element and spectral methods. The first discontinuous Galerkin (DG) method was introduced in 1973 by Reed and Hill [22], in the framework of neutron transport, i.e. a time independent linear hyperbolic equation. Then the complete discontinuous finite element basis have been analyzed in [15, 16] and used in the Runge-Kutta time stepping schemes [11]. These numerical schemes employ the piecewise discontinuous polynomials and also impose continuity weakly by penalizing the jump of solution across the element boundaries. Upwind schemes, first proposed as finite difference methods, were later extended to finite element methods to enforce the flux directions in [1, 3]. However, for problems with strong discontinuities, the DG scheme will involve significant oscillations near discontinuities. In such situation, the nonlinear limiters are needed to control these oscillations. In the previous work, minmod-based limiter [6, 7, 8, 9, 10], moment-based limiter [2, 4] have been developed. In [32], the simpler and compact higher order preserving limiter has been proposed for RKDG methods. In the target cell, the approximated polynomial is reconstructed depending on the information from the localized cell and the associated directly adjacent cells. The limiter reduces or even removes the spurious oscillations near discontinuities, and maintains the original high-order accuracy in smooth region. This limiter is later modified as a simple and compact Hermite WENO limiter [30] in order to improve the robustness in the computation of problems with strong shocks or contact discontinuities. Thanks to the compactness of the reconstruction stencil, such limiter is applied onto unstructured meshes [29, 31] and cubed sphere [14].

Weak Galerkin (WG) finite element method was first proposed by Wang and Ye in [25]. By using the discontinuous functions, WG schemes have the flexibilities in adopting general polytopal meshes and employing high order polynomials. This simple and parameter free formulation has been used to solve various partial differential equations, including convection-diffusion equations [17, 13], biharmonic problems [18], and Stokes flow [26, 27, 28], Burgers equations [5] etc. The upwind featured stabilizer methods are employed in [23] for steady hyperbolic equations.

In this work, we consider the time dependent hyperbolic equations. Our main purpose is to analyze the upwind weak Galerkin methods for time dependent hyperbolic equations both theoretically and numerically through this study. Then, this equation subject to discontinuous initial conditions may contain discontinuities for later solutions. Based on the proposed numerical schemes, we shall investigate the explicit time stepping method and the effective WENO limiter approach for generating the discontinuous capture feature capturing schemes. Because of the transient shock capturing feature, we extend the approach to investigate the inviscid Burgers equations. The rest of the paper is organized as follows: we introduce briefly the notations and finite element space in Section 2. In Section 3, the semi-discrete WG finite element method is proposed and analyzed. Section 4 is contributed to designing the explicit time stepping method and providing the details in WENO limiters. Then we discuss the applications of our scheme for solving Burgers equations. Numerical examples are presented in Section 5 for validating our theoretical conclusion and numerical performance. Lastly, the paper ends with conclusion and future research plans in Section 6.

2. Notations

In this section we shall introduce the notations, definitions necessary for proposing the weak Galerkin method.

Let $\mathcal{I}_h := \cup_{j=1}^{N}[x_{j-1}, x_j]$ be a partition of domain I, and $I_j = [x_{j-1}, x_j]$ be the partition element. Denote the mesh size by $h_j = x_j - x_{j-1}$ and $h = \max_j h_j$. For any given integer $k \geq 0$, the discrete weak function space associated with partition I_j is defined as following:

$$V_{I_j} = \{v = \{v_0, v_b^{j-1}, v_b^j\} : v_0 \in \mathbb{P}_k(I_j)\},$$

where $\mathbb{P}_k(I_j)$ denotes the polynomial with degree $\leq k$ on the interior of partition element I_j. Here $v_b^{j-1} := v_b|_{x_{j-1}}$ and $v_b^j := v_b|_{x_j}$ denote the endpoint values on the partition element $I_j = [x_{j-1}, x_j]$. For simplification of notations, we shall omit the superscript but denote v_b when there is no confusion. It is noted that the interior value v_0 may be independent of the endpoint values v_b^{j-1} and v_b^j. The weak Galerkin finite element space V_h is defined by

$$V_h = \{v = \{v_0, v_b\} : v \in \cup_{j=1}^{N} V_{I_j}, [\![v_b]\!]_{x_j} = 0, \forall j = 1, 2, \ldots, N-1\}. \tag{3}$$

Here the notation $[\![v]\!]|_{x_j} = v_b^{I_j}|_{x_j} - v_b^{I_{j-1}}|_{x_j}$. So in the finite element space v_b takes the single value on the grid point x_j $(j = 0, 1, \ldots, N)$, and v_0 is a piecewise polynomial with degree up to k. The subspaces with homogeneous boundary condition is denoted as $V_h^{0,\Gamma^+} := \{v \in V_h, v_b|_{\Gamma^+} = 0\}$ and $V_h^{0,\Gamma^-} := \{v \in V_h, v_b|_{\Gamma^-} = 0\}$.

Definition 1. For any $v = \{v_0, v_b\} \in V_h$, on each element $I_j = [x_{j-1}, x_j] \in \mathcal{I}_h$, the weak gradient is defined as $\mathrm{d}_w v \in \mathbb{P}_k(I_j)$ (integer $k \geq 0$) on I_j satisfying

$$\int_{I_j} \mathrm{d}_w v \; q dx = -\int_{I_j} v_0 \frac{dq}{dx} dx + v_b q|_{x_{j-1}}^{x_j}, \quad \forall q \in \mathbb{P}_k(I_j). \tag{4}$$

Throughout this paper we use standard notions for Sobolev spaces and their norms. Let T be a measurable set, then denote the inner product by $(\cdot,\cdot)_T$. The norm and semi-norm in the space $W^{m,2}(T)$ are denoted by $\|\cdot\|_{m,T}$ and $|\cdot|_{m,T}$. Denote $\|\cdot\|_T := \|\cdot\|_{0,T}$. Besides, if $T = I$, we shall withdraw the subscript T. For simplicity, we adopt the following notations,

$$\begin{aligned}
(v, w) &= \sum_{I_j \in \mathcal{I}_h} (v, w)_{I_j} = \sum_{I_j \in \mathcal{I}_h} \int_{I_j} vw dx, \\
\langle v, w\rangle &= \sum_{I_j \in \mathcal{I}_h} \langle v, w\rangle_{\partial I_j} = \sum_{I_j \in \mathcal{I}_h} \left(vw|_{x_{j-1}} + vw|_{x_j} \right).
\end{aligned}$$

The blinear form is introduced for $v, w \in V_h$, as following:

$$a(v, w) = \frac{1}{2}(\beta \mathrm{d}_w v, w_0) - \frac{1}{2}(\beta v_0, \mathrm{d}_w w) + S(v, w), \tag{5}$$

where

$$S(v, w) = \frac{1}{2}\langle |\beta|(v_0 - v_b), w_0 - w_b\rangle. \tag{6}$$

In the following of this paper, we use C for generic constants independent of mesh size, and the solution to equations (1)-(2), which may not necessarily be the same at each occurrence.

3. Semi-discrete WG finite element method

The goal of this section is to develop semi-discrete WG finite element method for problem (1)-(2) and derive error estimate in the discrete L^2-norm.

3.1. Semi-discrete WG finite element scheme

Based on the variational formulation, we propose the semi-discrete WG finite element method as following.

Algorithm 1. A weak Galerkin approximation for equation (1)-(2) is to seek $u_h(t) = \{u_0(t), u_b(t)\} \in V_h^{0,\Gamma^-}$ satisfying the following:

$$\begin{aligned} (\frac{\partial u_0}{\partial t}, v_0) + a(u_h, v) &= 0, \quad \forall v = \{v_0, v_b\} \in V_h^{0,\Gamma^+}, t \in J. && (7)\\ u_h(x,0) &= g_h(x), \quad x \in I. && (8) \end{aligned}$$

Here $g_h(x)$ is the projection for the initial condition $g(x)$ to the finite element space V_h.

Lemma 1. *There exists a unique numerical solution for the WG scheme (7)-(8).*

Proof. By the definition of bilinear form $a(\cdot,\cdot)$, for $\forall v \in V_h^{0,\Gamma^+}$

$$\begin{aligned} a(v,v) &= \frac{1}{2}(\beta \mathrm{d}_w v, v_0) - \frac{1}{2}(\beta \mathrm{d}_w v, v_0) + S(v,v)\\ &= S(v,v). \end{aligned}$$

Assume there exit two numerical solutions u_h^1 and u_h^2 for the above equation (7)-(8). By taking $\epsilon_h = u_h^1 - u_h^2$ and $v = \epsilon_h$, we get

$$\begin{aligned} 0 &= \frac{1}{2}\frac{d}{dt}\|\epsilon_0\|^2 + S(\epsilon_h, \epsilon_h)\\ &= \frac{1}{2}\frac{d}{dt}\|\epsilon_0\|^2 + \frac{1}{2}\sum_{I_j \in \mathcal{I}_h} \Big(\left[|\beta|(\epsilon_0 - \epsilon_b)^2\right]|_{x_{j-1}} + \left[|\beta|(\epsilon_0 - \epsilon_b)^2\right]|_{x_j} \Big). \end{aligned} \quad (9)$$

Since

$$(\epsilon_0 - \epsilon_b)|_{x_j}^2 \geq 0, j = 0, 1, \ldots, N,$$

we have

$$\frac{d}{dt}\|\epsilon_0\|^2 \leq 0.$$

Thanks to the fact $\|\epsilon_0\|^2 = 0$ at time $t = 0$, we conclude that $\|\epsilon_0\|^2 \equiv 0$, which implies uniqueness of the numerical solution to the scheme. Since the scheme (7)-(8) is posed in a finite dimensional space V_h^{0,Γ^-}, the uniqueness yields the existence of the solution. □

Besides, taking $v = u_h$ and following the same arguments, we obtain the L^2 stability as blow.

Lemma 2. *The solution $u_h = \{u_0, u_b\}$ to the semi-discrete WG scheme (7)-(8) satisfies the following L^2 stability.*

$$\frac{d}{dt}\|u_0\|^2 \leq 0.$$

Lemma 3. *The numerical solution of scheme (7)-(8) conserves mass.*

Proof. For simplicity, we assume $\beta > 0$ and thus the inflow boundary condition is given at grid point x_0, i.e, $u_b|_{x_0} = 0$ and $v_b|_{x_N} = 0$. Taking $v_0 = 1$ and $v_b|_{x_j} = 1, j = 0, \ldots, N-1$, $v_b|_{x_N} = 0$ in the equation (7), one gets

$$\frac{1}{2}\frac{d}{dt}\left(\sum_{I_j\in\mathcal{I}_h}\int_{I_j} u_0 dx\right) + T_1 - T_2 + T_3 = 0. \tag{10}$$

Here, the definition of weak gradient d_w and the boundary condition $u_b|_{x_0} = 0$ imply

$$\begin{aligned} T_1 &:= \frac{1}{2}(\beta \mathrm{d}_w u_h, v_0) = \frac{1}{2}\sum_{I_j\in\mathcal{I}_h}\int_{I_j}\beta \mathrm{d}_w u_h v_0 dx = \frac{1}{2}\sum_{I_j\in\mathcal{I}_h}\left(\beta u_b v_0|_{x_{j-1}}^{x_j} - \int_{I_j}\beta u_0\frac{\partial}{\partial x}1 dx\right) \\ &= \frac{1}{2}\sum_{I_j\in\mathcal{I}_h}(\beta u_b)|_{x_{j-1}}^{x_j} = -\frac{\beta}{2}u_b|_{x=x_0} + \frac{\beta}{2}u_b|_{x=x_N} = \frac{\beta}{2}u_b|_{x=x_N}. \end{aligned}$$

and by $v_0 = 1$, $v_b|_{x_j} = 1, j = 0, 1 \ldots, N-1$, $v_b|_{x_N} = 0$, and integration by parts, one obtains,

$$\begin{aligned} T_2 &:= \frac{1}{2}(\beta u_0, \mathrm{d}_w v) = \frac{1}{2}\sum_{I_j\in\mathcal{I}_h}\int_{I_j}\beta u_0 \mathrm{d}_w v dx = \frac{1}{2}\sum_{I_j\in\mathcal{I}_h}\left(\beta u_0 v_b|_{x_{j-1}}^{x_j} - \int_{I_j}\beta v_0\frac{\partial u_0}{\partial x}dx\right) \\ &= \frac{1}{2}\sum_{I_j\in\mathcal{I}_h}\left(\beta u_0 v_b|_{x_{j-1}}^{x_j} - \beta u_0|_{x_{j-1}}^{x_j}\right) = -\frac{\beta}{2}u_0|_{x_N}. \end{aligned}$$

Furthermore,

$$T_3 := S(u_h, v) = \frac{1}{2}\sum_{I_j\in\mathcal{I}_h}\langle|\beta|(u_0 - u_b), v_0 - v_b\rangle_{\partial I_j} = \frac{1}{2}\beta(u_0 - u_b)|_{x_N}.$$

Thus replacing the above estimates to (10), the following obtained

$$\frac{1}{2}\frac{d}{dt}\left(\sum_{I_j\in\mathcal{I}_h}\int_{I_j} u_0 dx\right) = 0,$$

which by taking integration completes the proof. □

Remark 4. The theoretical conclusions for homogeneous inflow boundary conditions also hold for periodic boundary conditions. The proof can be established in the same fashion.

3.2. Error Analysis

Let $Q_h : u \in H^1(I) \to Q_h u \in V_h$ such that $Q_h u|_{I_j} = \{Q_0 u, Q_b u\},\ j = 1, 2, \ldots, N$. Here Q_0 is the L^2-projection on the element I_j and Q_b denotes the interpolation of function u on the grids points x_j. It follows Bramble-Hilbert Lemma for projection operator that if $u \in H^{k+1}(I)$

$$\|Q_0 u - u\|_{I_j} + {h_j}^{k-1} |Q_0 u - u|_{1,I_j} \leq C {h_j}^k \|u\|_{k+1,I_j}. \tag{11}$$

Lemma 5. *Let $u \in H^1(I)$ and then for $q \in \mathbb{P}_k(I_j)$, $\forall I_j \in \mathcal{I}_h$*

$$(u_x, q)_{I_j} = (d_w Q_h u, q)_{I_j}. \tag{12}$$

Proof. By the definition of projection operator Q_h and the weak derivative d_w, one has

$$\begin{aligned} \int_{I_j} \mathrm{d}_w Q_h u q dx &= -\int_{I_j} Q_0 u \frac{\partial q}{\partial x} dx + [Q_b u q]_{x_j}^{x_{j+1}} = -\int_{I_j} u \frac{\partial q}{\partial x} dx + [uq]_{x_j}^{x_{j+1}} \\ &= \int_{I_j} \frac{\partial u}{\partial x} q dx \end{aligned}$$

and hence proves the lemma. □

Lemma 6. *Let $u(t) \in H^1(0, T; H^2(I))$ be the solution of problem (1)-(2). Then we have*

$$(\frac{\partial Q_0 u}{\partial t}, v_0) + a(Q_h u, v) = \ell_h(u, v) + S(Q_h u, v), \forall v \in V_h^0, t \in J, \tag{13}$$

where $\ell_h(u, v) = \dfrac{1}{2} \sum_{I_j \in \mathcal{I}_h} \beta (Q_0 u - Q_b u)(v_0 - v_b)|_{x_{j-1}}^{x_j}$.

Proof. Multiplying the equation (1) by v_0 and taking integration, we obtain

$$(\frac{\partial u}{\partial t}, v_0) + (\beta u_x, v_0) = 0. \tag{14}$$

It follows integration by parts and definitions of Q_0 and Q_b that

$$\begin{aligned} (\beta u_x, v_0)_{I_j} &= -\int_{I_j} \beta u \frac{\partial v_0}{\partial x} dx + \beta u v_0|_{x_{j-1}}^{x_j} = -\int_{I_j} \beta Q_0 u \frac{\partial v_0}{\partial x} dx + \beta Q_b u v_0|_{x_{j-1}}^{x_j} \\ &= \int_{I_j} \beta \frac{\partial Q_0 u}{\partial x} v_0 dx - \beta Q_0 u v_0|_{x_{j-1}}^{x_j} + \beta Q_b u v_0|_{x_{j-1}}^{x_j} \\ &= \int_{I_j} \beta \frac{\partial Q_0 u}{\partial x} v_0 dx - \beta Q_0 u v_b|_{x_{j-1}}^{x_j} + \beta Q_0 u (v_b - v_0)|_{x_{j-1}}^{x_j} + \beta Q_b u v_0|_{x_{j-1}}^{x_j} \\ &= -(\beta Q_0 u, \mathrm{d}_w v)_{I_j} + \beta Q_0 u (v_b - v_0)|_{x_{j-1}}^{x_j} + \beta Q_b u v_0|_{x_{j-1}}^{x_j}. \end{aligned}$$

Adding the above equation over j, together with $Q_b u|_{x_0} = 0, v_b|_{x_N} = 0$, and the fact $\sum_{I_j} \beta Q_b u v_b|_{x_{j-1}}^{x_j} = 0$, we get

$$(\beta u_x, v_0) = -(\beta Q_0 u, \mathrm{d}_w v) + \sum_{I_j \in \mathcal{I}_h} \beta (Q_0 u - Q_b u)(v_b - v_0)|_{x_{j-1}}^{x_j}. \tag{15}$$

Then Lemma 5 and (15) imply

$$\begin{aligned}(\beta u_x, v_0) &= \frac{1}{2}(\beta \mathrm{d}_w Q_h u, v_0) + \frac{1}{2}(\beta u_x, v_0) \\ &= \frac{1}{2}(\beta \mathrm{d}_w Q_h u, v_0) - \frac{1}{2}(\beta Q_0 u, \mathrm{d}_w v) + \frac{1}{2}\sum_{I_j \in \mathcal{I}_h} \beta(Q_0 u - Q_b u)(v_b - v_0)|_{x_{j-1}}^{x_j}\end{aligned}$$

and by substituting to equation (14) it follows,

$$(\frac{\partial u}{\partial t}, v_0) + \frac{1}{2}(\beta \mathrm{d}_w Q_h u, v_0) - \frac{1}{2}(\beta Q_0 u, \mathrm{d}_w v) + \frac{1}{2}\sum_{I_j \in \mathcal{I}_h} \beta(Q_0 u - Q_b u)(v_b - v_0)|_{x_{j-1}}^{x_j} = 0.$$

Adding $S(Q_h u, v)$ to both sides gives the conclusion. □

Thus, subtracting (7) from (13), and denote $e_h = Q_h u - u_h$, we have the following error equation:

$$(\frac{\partial e_0}{\partial t}, v_0) + a(e_h, v) = \ell_h(u, v) + S(Q_h u, v), \forall v \in V_h^{\Gamma^+, 0}. \tag{16}$$

Theorem 7. *Let $u(x,t)$ and $u_h(x,t) = \{u_0(x,t), u_b(x,t)\}$ be the solutions of problem (1)-(2) and (7)-(8), respectively, with $u \in H^1(0,T; H^{1+k}(I))$ and $g_h = Q_h g$. Then, there exists a constant C such that*

$$\|Q_0 u - u_0\|^2 \leq C h^{2k+1} \int_0^t \|u\|_{k+1}^2 ds. \tag{17}$$

Proof. By triangle inequality, one obtains,

$$\|Q_0 u - Q_b u\|_{\partial I_j} \leq \|Q_0 u - u\|_{\partial I_j} + \|u - Q_b u\|_{\partial I_j}.$$

The fact that $Q_b u$ denotes the interpolation of function u on the grid points gives

$$\|Q_0 u - Q_b u\|_{\partial I_j} \leq \|Q_0 u - u\|_{\partial I_j}.$$

Such bound, together with Cauchy-Schwartz inequality, trace inequality, and Young's inequality, one has

$$\begin{aligned}\ell_h(u, e_h) &= \frac{1}{2}\sum_{I_j \in \mathcal{I}_h} (\beta(Q_0 u - Q_b u), e_0 - e_b)|_{x_{j-1}}^{x_j} \\ &\leq \sum_{I_j \in \mathcal{I}_h} \|Q_0 u - Q_b u\|_{\partial I_j} \||\beta|(e_0 - e_b)\|_{\partial I_j} \\ &\leq \sum_{I_j \in \mathcal{I}_h} \|Q_0 u - u\|_{\partial I_j} \||\beta|(e_0 - e_b)\|_{\partial I_j} \\ &\leq C h^{k+1/2} \sum_{I_j \in \mathcal{I}_h} \|u\|_{k+1, I_j} \||\beta|(e_0 - e_b)\|_{\partial I_j} \\ &\leq C h^{2k+1} \|u\|_{k+1}^2 + \frac{1}{4}\sum_{I_j \in \mathcal{I}_h} \||\beta|(e_0 - e_b)\|_{\partial I_j}^2.\end{aligned}$$

Cauchy-Schwartz inequality and Young's inequality imply

$$\begin{aligned} S(Q_h u, e_h) &\leq C \sum_{I_j \in \mathcal{I}_h} \|Q_0 u - Q_b u\|_{\partial I_j} \||\beta|(e_0 - e_b)\|_{\partial I_j} \\ &\leq Ch^{2k+1} \|u\|_{k+1}^2 + \frac{1}{4} \sum_{I_j \in \mathcal{I}_h} \||\beta|(e_0 - e_b)\|_{\partial I_j}^2. \end{aligned}$$

By the formulation of bilinear form $a(\cdot, \cdot)$, $a(e_h, e_h) = S(e_h, e_h)$, and thus (16) can be re-written as

$$\begin{aligned} \frac{\partial}{\partial t}\|e_0\|^2 + S(e_h, e_h) &= \frac{\partial}{\partial t}\|e_0\|^2 + \frac{1}{2} \sum_{I_j \in \mathcal{I}_h} \||\beta|(e_0 - e_b)\|_{\partial I_j}^2 \\ &= \ell_h(u, e_h) + S(Q_h u, e_h) \\ &\leq Ch^{2k+1} \|u\|_{k+1}^2 + \frac{1}{2} \sum_{I_j \in \mathcal{I}_h} \||\beta|(e_0 - e_b)\|_{\partial I_j}^2. \end{aligned}$$

One obtains

$$\frac{\partial}{\partial t}\|e_0\|^2 \leq Ch^{2k+1} \|u\|_{k+1}^2.$$

Integrating the above estimate with respect to t and together with Gronwall lemma, we can get the following estimate

$$\|e_0\|^2 \leq Ch^{2k+1} \int_0^t \|u\|_{k+1}^2 ds.$$

4. Implementation Details

In this section, we shall discuss the implementation details for fully-discrete WG finite element method for problem (1)-(2). Denote the basis functions corresponding to v_0 as Φ_j and v_b as Ψ_j; the coefficient vectors corresponding to u_0 and u_b are denoted as $\mathbf{U_0}$ and $\mathbf{U_b}$ The algorithm can be reformed as following matrix form:

$$\begin{pmatrix} \mathbb{M}\dfrac{\partial}{\partial t}\mathbf{U_0} \\ \mathbb{0} \end{pmatrix} + \begin{bmatrix} \mathbb{A}_{00} & \mathbb{A}_{0b} \\ \mathbb{A}_{b0} & \mathbb{A}_{bb} \end{bmatrix} \begin{pmatrix} \mathbf{U}_0 \\ \mathbf{U}_b \end{pmatrix} = 0, \tag{18}$$

where the matrix $\mathbb{M} = \sum_{I_j} (\Phi_m, \Phi_n)_{I_j}$ denote the mass matrix and the matrices $\mathbb{A}_{00} = a(\Phi_m, \Phi_n)$, $\mathbb{A}_{0b} = a(\Phi_m, \Psi_n)$, $\mathbb{A}_{b0} = a(\Psi_m, \Phi_n)$ and $\mathbb{A}_{bb} = a(\Psi_m, \Psi_n)$ ($m = 1, \ldots, \#\text{DoF}_{u_0}$ and $n = 1, \ldots, \#\text{DoF}_{u_b}$). In this paper, we shall consider implicitbackward Euler's method, explicit forward Euler's method, and third order TVD Runge-Kutta's method.

4.1. Implicit Time Stepping Method

The implicit time stepping method has to take an inversion of a big matrix at each time step. For example, let assume the backward Euler's method. Denote the time step as τ and denote $\mathbf{U}^{n+1} = [\mathbf{U}_0^{n+1}, \mathbf{U}_b^{n+1}]^\top$. The time derivative is replaced by $\dfrac{\partial}{\partial t}\mathbf{U} = \dfrac{\mathbf{U}^{n+1} - \mathbf{U}^n}{\tau}$ and we are solving the following system:

$$\begin{pmatrix} \dfrac{\mathbb{M}\mathbf{U}_0^{n+1} - \mathbb{M}\mathbf{U}_0^n}{\tau} \\ \mathbb{0} \end{pmatrix} + \begin{bmatrix} \mathbb{A}_{00} & \mathbb{A}_{0b} \\ \mathbb{A}_{b0} & \mathbb{A}_{bb} \end{bmatrix} \begin{pmatrix} \mathbf{U}_0^{n+1} \\ \mathbf{U}_b^{n+1} \end{pmatrix} = 0.$$

4.2. Explicit Time Stepping Method

The explicit time stepping method is first to solve u_b from u_0 from all the test functions v_b as follows,

$$\mathbf{U}_b = -\mathbb{A}_{bb}^{-1}\mathbb{A}_{b0}\mathbf{U}_0. \tag{19}$$

Substituting the above equation (19) to (18), and the equations can be rewritten as:

$$\mathbb{M}\frac{\partial}{\partial t}\mathbf{U}_0 + \mathbb{A}_{00}\mathbf{U}_0 + \mathbb{A}_{0b}\Big(- \mathbb{A}_{bb}^{-1}\mathbb{A}_{b0}\mathbf{U}_0 \Big) = 0.$$

Rearranging the above equation, one has

$$\mathbb{M}\frac{\partial}{\partial t}\mathbf{U}_0 + (\mathbb{A}_{00} - \mathbb{A}_{0b}\mathbb{A}_{bb}^{-1}\mathbb{A}_{b0})\mathbf{U}_0 = 0. \tag{20}$$

For simplicity, denote $\mathbb{K} = -(\mathbb{A}_{00} - \mathbb{A}_{0b}\mathbb{A}_{bb}^{-1}\mathbb{A}_{b0})$, then we can rewritten the equation (20) to

$$\mathbb{M}\frac{\partial}{\partial t}\mathbf{U}_0 - \mathbb{K}\mathbf{U}_0 = 0. \tag{21}$$

The above ODE system $\dfrac{\partial}{\partial t}\mathbf{U}_0 = \mathbb{M}^{-1}\mathbb{K}\mathbf{U}_0 := L(\mathbf{U}_0)$ can be solved by explicit forward Euler's method or the following third order TVD Runge-Kutta (RK3) method given by

$$\begin{aligned} \mathbf{U}_0^{(1)} &= \mathbf{U}_0^n + \Delta t L(\mathbf{U}_0^n), \\ \mathbf{U}_0^{(2)} &= \frac{3}{4}\mathbf{U}_0^n + \frac{1}{4}\mathbf{U}_0^{(1)} + \frac{1}{4}\Delta t L(\mathbf{U}_0^{(1)}), \\ \mathbf{U}_0^{n+1} &= \frac{1}{3}\mathbf{U}_0^n + \frac{2}{3}\mathbf{U}_0^{(2)} + \frac{2}{3}\Delta t L(\mathbf{U}_0^{(2)}). \end{aligned}$$

4.3. WENO limiter

In this subsection, we cite the details of the WENO limiting procedure in [32] and modify it for our method.

The schemes to solve hyperbolic equations with possibly discontinuous solutions suffer oscillatory numerical results near the discontinuities, which may lead to instability and cause the

simulation to blow up. The goal for applying WENO limiter is to reduce the spurious oscillations of numerical solutions near discontinuities and maintain the original high order accuracy of the scheme in smooth region. It is achieved by detecting the troubled cells, and then reconstructing the approximation on interior of the troubled cell from a local stencil (including the cell and its immediate neighboring cells). The reconstruction is a convex combination of three candidates, including the original solution and the two modified extrapolations from neighbor cells. The weights in this reconstruction are determined by smoothness of the candidates. Such reconstructions are only applied onto the troubled cells to save computational cost and also protect the accuracy in the smooth region. We adopt the following framework:

Algorithm 2. The WENO limiting procedure is described as follows. Assuming that WG solution at time step n is u_h^n, for cells $I_j, j = 1, \ldots, N$,

1. Use the minmod limiter described in (22) and (25) to detect whether I_j is a troubled cell or not.
2. If I_j is not a troubled cell, then $u_0^{n,\text{new}}|_{I_j} = u^n|_{I_j}$.
3. If I_j is a troubled cell, then
   (a) Denote u_0^n on the cells I_{j-1}, I_j, I_{j+1} as $p_0(x), p_1(x), p_2(x)$, respectively, and modify $p_0(x), p_2(x)$ to $\tilde{p}_0(x), \tilde{p}_2(x)$ using (26) to get correct cell averages.
   (b) Compute the normalized nonlinear weights ω_l using (28) and (29) for $l = 0, 1, 2$.
   (c) The reconstruction polynomial is given by $u_0^{n,\text{new}}|_{I_j} = \omega_0\tilde{p}_0(x) + \omega_1 p_1(x) + \omega_2\tilde{p}_2(x)$.
4. The boundary elements $u_b^{n,\text{new}}$ will be updated by solving from $u_0^{n,\text{new}}$, if any trouble cell exits.

4.3.1. Identify the troubled cells

The detection of trouble cells uses a minmod function, defined by

$$m(a_1, \ldots, a_l) = \begin{cases} s \min_{1\le j\le l} |a_j|, & \text{if } s = \text{sign}(a_1) = \cdots = \text{sign}(a_l), \\ 0, & \text{otherwise.} \end{cases} \tag{22}$$

with variation information at both cell boundaries.

Denote the cell average of the solution u as

$$\bar{u}_j = \frac{1}{h_j}\int_{I_j} u dx \tag{23}$$

and the variation at the cell boundaries are denoted as

$$\tilde{u}_j = u(x_j^-) - \bar{u}_j \text{ and } \tilde{\tilde{u}}_j = \bar{u}_j - u(x_{j-1}^+). \tag{24}$$

Now we check

$$\tilde{u}_j^{(\text{mod})} = m(\tilde{u}_j, \Delta_+\bar{u}_j, \Delta_-\bar{u}_j), \quad \tilde{\tilde{u}}_j^{(\text{mod})} = m(\tilde{\tilde{u}}_j, \Delta_+\bar{u}_j, \Delta_-\bar{u}_j), \tag{25}$$

with the cell average jumps

$$\Delta_+\bar{u}_j = \bar{u}_{j+1} - \bar{u}_j, \quad \Delta_-\bar{u}_j = \bar{u}_j - \bar{u}_{j-1}.$$

The minmod function in (25) gets enacted and returns other than the first argument, only if the variation and cell average jumps have different signs, or the variation is more significant than cell average jumps. In this case, we claim it is a troubled cell, and subject to WENO reconstructions. We refer the readers to [19] about the comparison among different troubled-cell indicators and some new approaches [12, 24, 20, 21].

4.3.2. WENO reconstruction of the new polynomials in the troubled cells

The idea is to reconstruct the solution on troubled cell with a convex combination of polynomials on this cell and its immediate neighboring cells. To keep the original cell average on the target cell, some constant adjustments are needed.

Assume that the cell I_j is a troubled cell. Denote the WG solution polynomial of u_0 on the cells I_{j-1}, I_j, I_{j+1} as $p_0(x)$, $p_1(x)$, and $p_2(x)$, respectively. The polynomials $p_0(x)$, and $p_2(x)$ are modified by a constant as follows:

$$\tilde{p}_0(x) = p_0(x) - \bar{p}_0 + \bar{p}_1, \quad \tilde{p}_2(x) = p_2(x) - \bar{p}_2 + \bar{p}_1, \tag{26}$$

where

$$\bar{p}_0 = \frac{1}{h_j}\int_{I_j} p_0(x)dx, \quad \bar{p}_1 = \frac{1}{h_j}\int_{I_j} p_1(x)dx, \quad \bar{p}_2 = \frac{1}{h_j}\int_{I_j} p_2(x)dx.$$

The nonlinear WENO reconstruction polynomial $p_1^{\text{new}}(x)$ is defined by a convex combination of these modified polynomials:

$$p_1^{\text{new}}(x) = \omega_0\tilde{p}_0(x) + \omega_1 p_1(x) + \omega_2\tilde{p}_2(x), \tag{27}$$

where the weights w_0, w_1 and w_2 are non-negative and yet to be determined. It is easy to prove that p_1^{new} has the same cell average and order of accuracy as p_1 if the weights satisfy $\omega_0 + \omega_1 + \omega_2 = 1$.

The normalized nonlinear weights are defined as,

$$\omega_0 = \frac{\bar{\omega}_0}{\bar{\omega}_0 + \bar{\omega}_1 + \bar{\omega}_2}, \ \omega_1 = \frac{\bar{\omega}_1}{\bar{\omega}_0 + \bar{\omega}_1 + \bar{\omega}_2}, \ \omega_2 = \frac{\bar{\omega}_2}{\bar{\omega}_0 + \bar{\omega}_1 + \bar{\omega}_2}, \tag{28}$$

where the non-normalized nonlinear weights $\bar{\omega}_j$ $(j = 0, 1, 2)$ are functions of the positive linear weights γ_j and the so-called smoothness indicators β_j as follows:

$$\bar{\omega}_j = \frac{\gamma_j}{(10^{-6} + \beta_j)^2}, \text{ where } \beta_j = \sum_{\ell=1}^{k}\int_{I_j} h_j^{2\ell-1}\left[\frac{\partial^\ell}{\partial x^\ell}p_j(x)\right]^2 dx. \tag{29}$$

In general we put larger weight on the central cell, i.e., $\gamma_1 \gg \gamma_0$ and $\gamma_1 \gg \gamma_2$, since it is usually the best for smooth functions. In the numerical tests we take

$$\gamma_0 = 0.001, \gamma_1 = 0.998, \gamma_2 = 0.001,$$

which can maintain the original high order in smooth regions and can keep essentially nonoscillatory shock transition.

5. Applications in Burgers Equations

The numerical scheme can be extended to nonlinear hyperbolic equation, for example the inviscid Burgers equations. The Burgers equations considered in this paper is described as follows:

$$\begin{aligned} \frac{\partial u}{\partial t} + u\frac{\partial u}{\partial x} &= 0, \quad (x,t) \in I \times J \qquad (30) \\ \mathcal{B}u &= 0, \quad x \in \Gamma, \qquad (31) \end{aligned}$$

with initial condition $u(x,0) = h(x)$, where $\mathcal{B}$ is the operator for boundary conditions. We consider both periodic boundary conditions $u(a,t) = u(b,t)$ for domain $I = [a,b]$, and Dirichlet boundary conditions $u(a,t) = h_1(t)$ and $u(b,t) = h_2(t)$. Denote $H^1_{\mathcal{B},\Gamma}(I)) = \{u \in H^1(I) : \mathcal{B}u = 0\}$.

The weak form for problem (30)-(31) is to find $u \in H^1_{\mathcal{B},\Gamma}(I))$, such that

$$(u_t, v) + \frac{1}{3}(uu_x, v) - \frac{1}{3}(uu, v_x) = 0, \quad \forall v \in H^1(I), t \in (0,T] \qquad (32)$$

and $u(x,0) = h(x), x \in I$.

Similarly as the bilinear form for hyperbolic equation, here we introduce the trilinear form for $w, u, v \in V_h$, as following:

$$B(w;u,v) = \frac{1}{3}(w\mathrm{d}_w u, v_0) - \frac{1}{3}(u_0, w\mathrm{d}_w v) + S_{\text{Burgers}}(w;u,v), \qquad (33)$$

where

$$S_{\text{Burgers}}(w;u,v) = \frac{1}{3}\langle |w_0|(u_0 - u_b), v_0 - v_b\rangle. \qquad (34)$$

Denote the approximation space $V_h^{\mathcal{B}} = \{u \in V_h : \mathcal{B}u = 0\}$ and the space for test function as V_h^T. For periodic boundary condition,

$$V_h^{\mathcal{B}} := \{u = \{u_0, u_b\} \in V_h : u_b|_a - u_b|_b = 0\},$$

and the space for test function is also $V_h^T = V_h^{\mathcal{B}}$; and for Dirichlet boundary condition,

$$V_h^{\mathcal{B}} := \{u = \{u_0, u_b\} \in V_h : u_b|_a = h_1(t), \text{and } u_b|_b = h_2(t)\},$$

and $V_h^T = V_h$. Then the semi-discrete WG scheme is proposed for Burgers equation as below.

Algorithm 3. A weak Galerkin approximation for equation (30)-(31) is to seek $u_h = \{u_0, u_b\} \in V_h^{\mathcal{B}}$ satisfying the following:

$$\begin{aligned} (\frac{\partial u_0}{\partial t}, v_0) + B(u_0; u_h, v) &= 0, \qquad \forall v = \{v_0, v_b\} \in V_h^T. \qquad (35) \\ u_h(x,0) &= Q_h h(x), \quad x \in I. \qquad (36) \end{aligned}$$

Lemma 8. *The solution $u_h = \{u_0, u_b\}$ to the semi-discrete WG scheme (35)-(36) satisfies the following L^2-stability.*

$$\frac{d}{dt}\|u_0\|^2 \le 0.$$

PROOF. By the definition of trilinear form $a(\cdot,\cdot)$, for $\forall v \in V_h^T$

$$\begin{aligned} B(v;v,v) &= \frac{1}{3}(v_0 \mathrm{d}_w v, v_0) - \frac{1}{3}(v_0 \mathrm{d}_w v, v_0) + S_{\text{Burgers}}(v;v,v) \\ &= S_{\text{Burgers}}(v;v,v). \end{aligned}$$

By taking $v = u_h$, we get

$$\begin{aligned} 0 &= \frac{1}{2}\frac{d}{dt}\|u_0\|^2 + S_{\text{Burgers}}(u_h;u_h,u_h) \\ &= \frac{1}{2}\frac{d}{dt}\|u_0\|^2 + \frac{1}{3}\sum_{I_j \in \mathcal{I}_h} \left(\left[|u_0|(u_0-u_b)^2\right]|_{x_{j-1}} + \left[|u_0|(u_0-u_b)^2\right]|_{x_j} \right). \end{aligned} \tag{37}$$

Since

$$|u_0|(u_0-u_b)^2|_{x_j} \geq 0, j = 0, 1, \ldots, N,$$

we have

$$\frac{d}{dt}\|u_0\|^2 \leq 0,$$

which completes the proof. □

In the fully discretized numerical scheme, we use the previous solution u_0 to linearize the trilinear term $B(u_0;u_h,v)$ by $B(u_0^{n-1};u_h^n,v)$ to solve for u_h^n.

6. Numerical Test

In this section, we shall report the numerical performance of the proposal scheme. Eight numerical experiments shall be tested to validate our numerical scheme. Although only the sub-optimal convergence can be proved in Theorem 7, one can observe the optimal rate in convergence for both linear convection equation and Burgers equation.

6.1. Convergence Test for Linear Convection Equation

In this test, we shall validate the theoretical conclusion for the WG algorithm. Let $I = [0, 2\pi]$, $\beta = 1$, and the exact solution is chosen as $u = \exp(-t)\sin(x)$. The time discretization is performed by 3rd order TVD Runge-Kutta method with $\Delta t = 10^{-4}$. We calculate the numerical solution up to time $T = 0.01$. The error profiles and convergence results are reported in Table 1. As shown in this table, we achieve the optimal rate in convergence for errors measured in L^2 and H^1 norms, which are at the order $\mathcal{O}(h^{k+1})$ and $\mathcal{O}(h^k)$.

Table 1: Example 6.1: Error profiles and convergence results.

$1/h$	Relative L^2-Error	Order	Relative H^1-Error	Order
		$k=0$		
10	2.6262E-01		1.0000E+00	
20	1.0556E-01	1.31	1.0000E+00	-
40	4.8793E-02	1.11	1.0000E+00	-
80	2.3537E-02	1.05	1.0000E+00	-
160	1.1562E-02	1.03	1.0000E+00	-
		$k=1$		
10	9.4438E-02		3.0025E-01	
20	1.3729E-02	2.78	1.0825E-01	1.47
40	2.6776E-03	2.36	4.8933E-02	1.15
80	6.2248E-04	2.10	2.4281E-02	1.01
160	1.5652E-04	1.99	1.2567E-02	0.95
		$k=2$		
10	1.6589E-03		1.5317E-02	
20	1.9020E-04	3.12	3.8428E-03	1.99
40	2.2934E-05	3.05	1.0239E-03	1.91
80	3.0247E-06	2.92	2.5573E-04	2.00
160	4.0292E-07	2.91	6.3270E-05	2.02

6.2. WENO Limiter for Linear Convection Equation

In this test, we shall choose $I = [0, 1]$, $\beta = 1$, and the following initial condition for the unsteady linear convection equation in (1):

$$u(x, t = 0) = H(0, 2) - H(0.4) \tag{38}$$

where H represents the Heaviside step function. The boundary condition for this case is set to be homogeneous inflow boundary condition. The step function will move along x-axis to the right as time envolves. However, the discontinuities may develop oscillations in the numerical solution.

Case 6.2a. Performance of WG algorithm.

First, we shall present the numerical performance of the proposed WG scheme with different polynomial orders. Let $h = 1/100$ and the time integration is carried out using a simple forward Euler scheme with time step $\Delta t = 10^{-4}$.

The numerical solutions for different WG elements are plotted in Figure 1. The solid line and dotted line plot the numerical solutions at time = 0.1 and time = 0.2, respectively. As one can see that the solution of this linear advection equation is a step function moves to the right. However, the numerical solutions with $k \geq 1$ show oscillations at the location with discontinuities. Increasing the degree of polynomial does not improve the simulations, but leads to more oscillations. In order to improve the numerical performance, one has to increase resolution of the spatial variable for resolving such discontinuities.

The values of mass (computed as: $\text{Mass}(t) = \sum_j \int_{I_j} |u_0(x,t)|dt$) and energy (computed as: $\text{Energy}(t) = \sum_j \int_{I_j} |u_0(x,t)|^2 dt$) are plotted in Figure 2. It can be observed that the mass is well conserved for all the WG elements. However, the quantity of energy is well conserved except constant WG element. Besides, for $k = 0$, the discontinuity in the numerical solution is smoothed out, as shown in Figure 1(a), which is poor approximation.

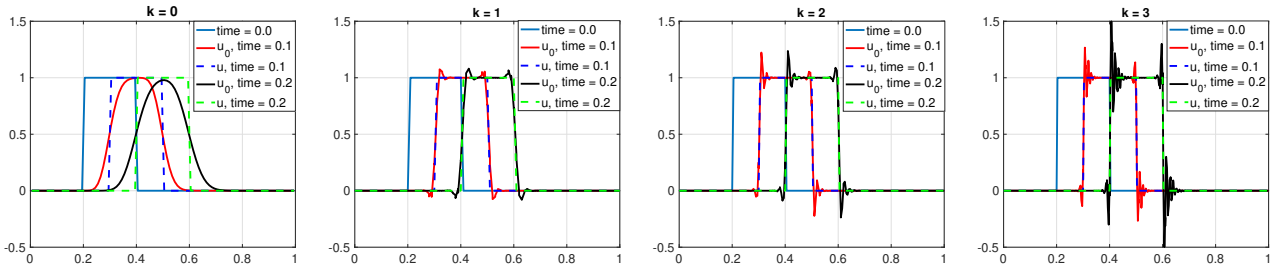

(a) (b) (c) (d)

Figure 1: Example 6.2a: Plot of numerical solution for WG element on $h = 0.01$ with: (a) $k = 0$; (b) $k = 1$; (c) $k = 2$; (d) $k = 3$. In all the figures, the solid lines denote the numerical solutions and the dotted lines denote the exact solutions.

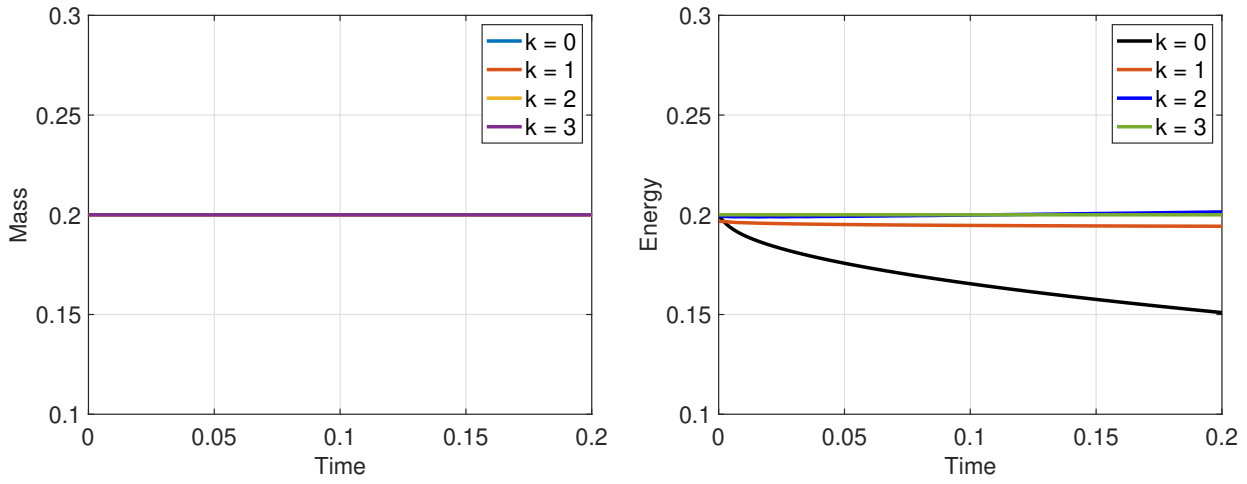

(a) (b)

Figure 2: Example 6.2a: Plots of WG approximation properties on mesh $h = 0.01$ with various WG elements for (a) mass; (b) energy.

Case 6.2b. Performance of WENO Limiter

Due to the possible oscillation in the linear advection equation's approximation, the WENO limiter can be applied for filtering out the oscillation around discontinuities. This test is conducted to validate the effectiveness for WENO limiter.

The time integration is carried out using the third order TVD Runge-Kutta method with time step $\Delta t = 10^{-3}$ and the numerical solutions are plotted in Figure 3 for WG element $k = 1$, $k = 2$, and $k = 3$. Comparing to forward Euler scheme, shown in Figure 1, by purely increasing the

accuracy in time stepping method cannot generate the oscillation-free solutions. Besides, higher order WG element may results in more oscillations.

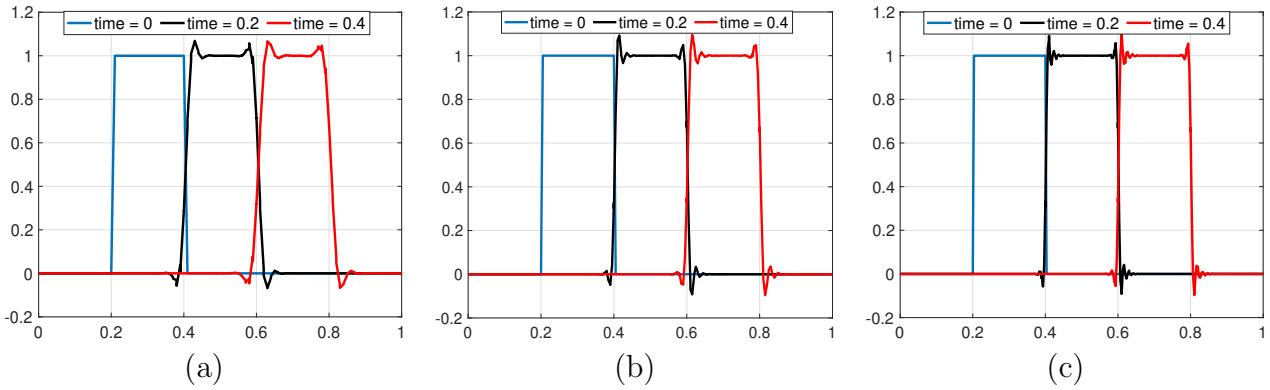

Figure 3: Example 6.2b: Plot of numerical solution on mesh $h = 0.01$ with for WG elements (a) $k = 1$; (b) $k = 2$; (c) $k = 3$.

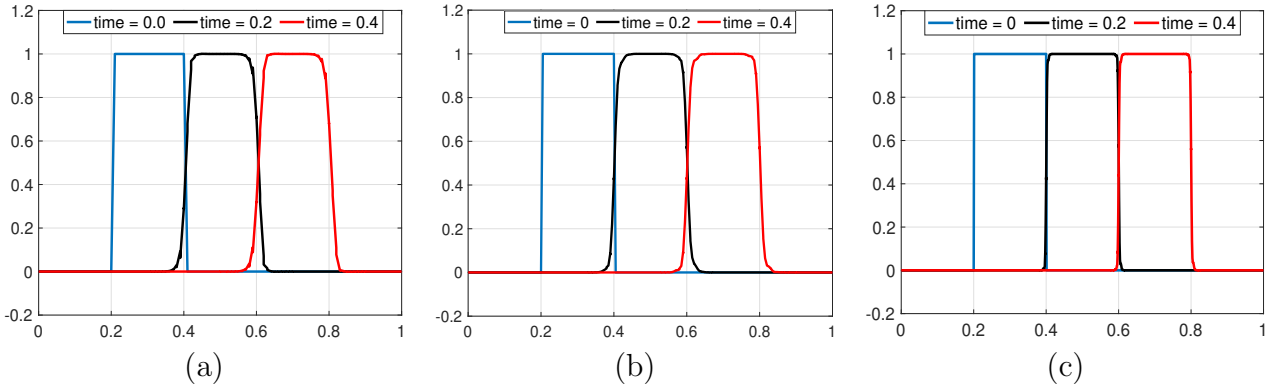

Figure 4: Example 6.2b: Plot of numerical solution on mesh $h = 0.01$ with WENO limiter for WG elements (a) $k = 1$; (b) $k = 2$; (c) $k = 3$.

In order to improve the numerical simulation, we shall employ the WENO limiter as Algorithm 2. The numerical solutions for WG with WENO limiter on the same mesh with $h = 0.01$ and $\Delta t = 10^{-3}$ for WG element $k = 1$, $k = 2$, and $k = 3$ are plotted in Figure 4. It can be observed that after employing the limiter, the oscillations near discontinuity have been cleared. By using higher order WG element, the sharp discontinuity can be well captured. Besides, the mass corresponding to the scheme with limiter and without limiter for $k = 1$ is plotted in Figure 5. It is noted that adding limiter maintains the mass conservation of WG scheme.

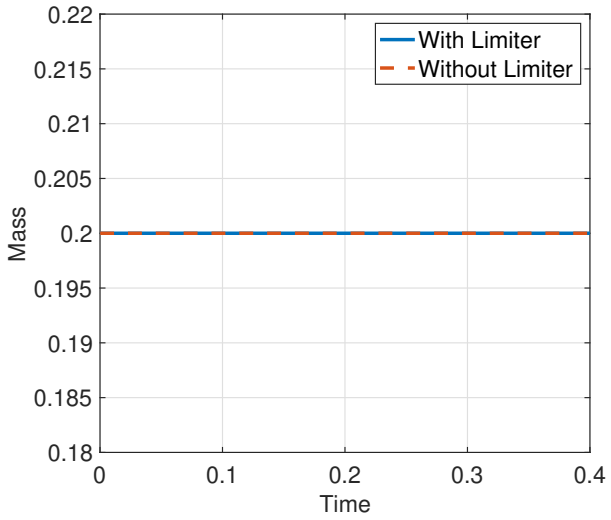

Figure 5: Example 6.2b: illustration of mass for the mesh with $h = 0.01$ and $k = 1$.

6.3. Convergence Test for Burgers Equation

Table 2: Example 6.3: Error profiles and convergence results.

$1/h$	Relative L^2-Error	Order	Relative H^1-Error	Order
		$k = 0$		
10	9.0626E-02		1.0000E+00	-
20	4.5336E-02	1.00	1.0000E+00	-
40	2.2671E-02	1.00	1.0000E+00	-
80	1.1336E-02	1.00	1.0000E+00	-
160	5.6682E-03	1.00	1.0000E+00	-
		$k = 1$		
10	9.0009E-03		9.0579E-02	-
20	2.2561E-03	2.00	4.5399E-02	1.00
40	5.6618E-04	1.99	2.2800E-02	0.99
80	1.4304E-04	1.98	1.1544E-02	0.98
160	1.8700E-05	2.94	5.9401E-03	0.96
		$k = 2$		
10	1.7818E-04		3.6759E-03	-
20	2.2297E-05	3.00	9.2196E-04	2.00
40	2.7890E-06	3.00	2.3257E-04	1.99
80	3.5043E-07	2.99	6.0037E-05	1.95
160	4.5138E-08	2.96	1.5503E-05	1.95

In this test, we shall validate the convergence results for the Burgers equations. Let $I = [0, 2\pi]$ and the source term is added such that the equation is satisfied for choosing the exact solution as

$$u = e^{-t} \sin \pi x.$$

The time discretization is replaced by 3rd order TVD Runge-Kutta method. We perform the WG simulation on different size of the meshes. Here $\Delta t = 10^{-5}$ is chosen sufficient small in order to not affect the convergence rate. The explicit time stepping methods are calculated up to time $= 0.01$. The error profiles and convergence test are reported in Table 2. It shows that the relative L^2-error converges at the order $\mathcal{O}(h^{k+1})$ and the relative H^1-error converges at the order $\mathcal{O}(h^k)$.

6.4. Burgers 1D: Smooth initial profile for steady shock

In this case, let $I = [0, 1]$ and the initial condition is set to be a sinusoidal profile

$$u(x, t = 0) = \sin(2\pi x) \tag{39}$$

and the boundary conditions are homogeneous Dirichlet at both ends of the domain.

This set of conditions yields a solution that initially develops into a steady shock due to the initial condition and dies off. In this test, the time integration is carried out using a backward Euler with $\Delta t = 10^{-4}$. The numerical solution corresponding to mesh with $h = 0.01$ and $k = 2$ is plotted in Figure 6. Because the discontinuity is located on the grid point, the numerical scheme without WENO limiter can approximate the problem without oscillation very well.

In this test, since the problem is with steady shock, so it is possible to generate the well fitted mesh. However, for most of Burgers equation, generating such mesh is impossible.

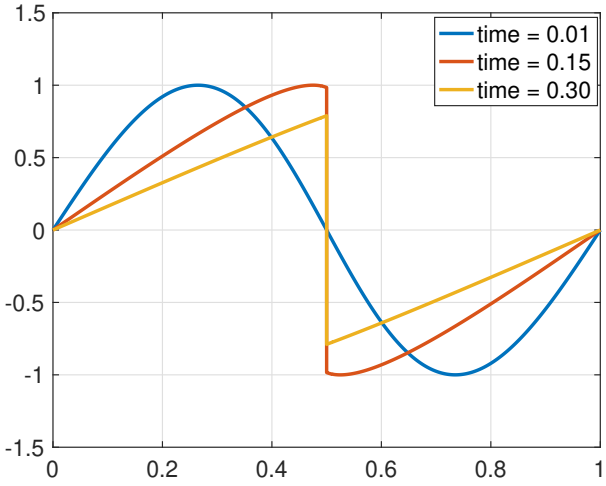

Figure 6: Example 6.5: Numerical solution for WG scheme for $k = 2$ and $h = 0.01$.

6.5. Burger's equation: smooth initial condition

Let $I = [0, 1]$ and consider the following smooth initial condition:

$$u(0) = \exp(-200(x - 0.3)^2). \tag{40}$$

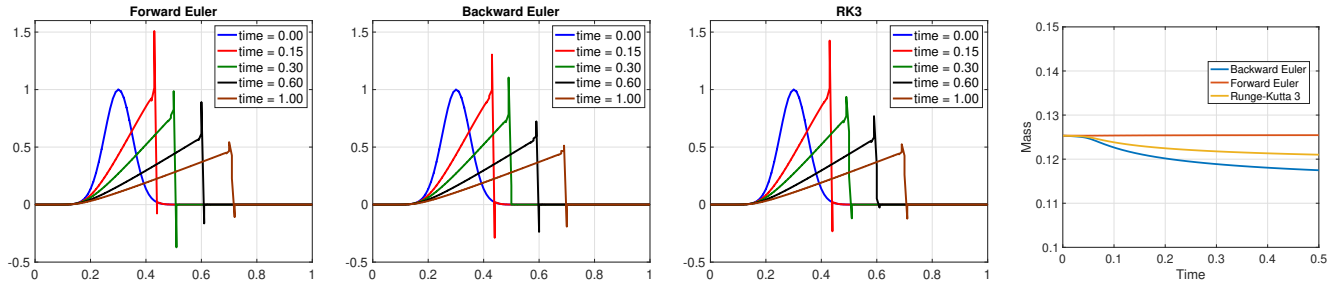

(a) (b) (c) (d)

Figure 7: Example 6.5: Numerical solution of $h = \frac{1}{100}, \Delta t = 10^{-3}$ and $k = 1$ for (a) Forward Euler method; (b) Backward Euler method; (c) Third order Runge-Kutta method; (d) Plot of Mass.

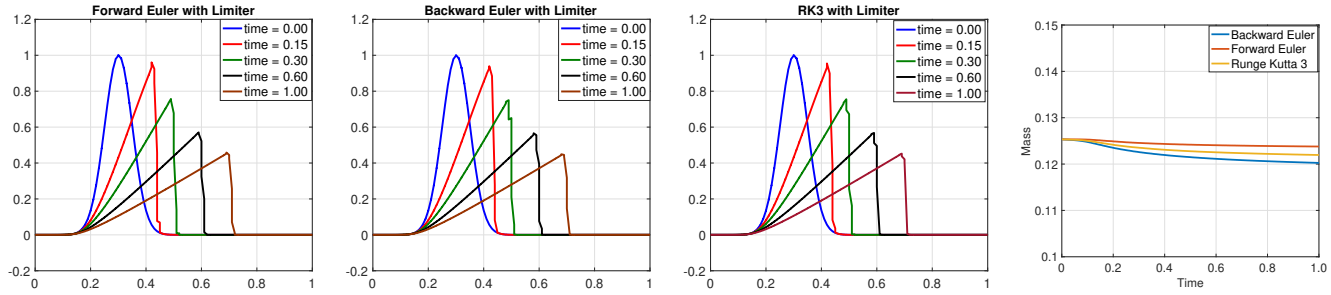

(a) (b) (c) (d)

Figure 8: Example 6.5: Numerical solution of $h = \frac{1}{100}, \Delta t = 10^{-3}$ and $k = 1$ with WENO limiter for (a) Forward Euler method; (b) Backward Euler method; (c) Third order Runge-Kutta method; (d) Plot of Mass.

Different time discretization schemes have been used in the simulation, including forward Euler method, backward Euler method, and RK3 method. The results for linear WG element on the mesh with $h = 0.01$ and $\Delta t = 10^{-3}$ are plotted in Figure 7 without limiter and Figure 8 with limiter. As one can observe that the simulations without limiter show oscillations near discontinuities, while by adding limiter in the scheme can significantly clear the oscillations. Besides, the forward Euler scheme shows the best mass conservation property.

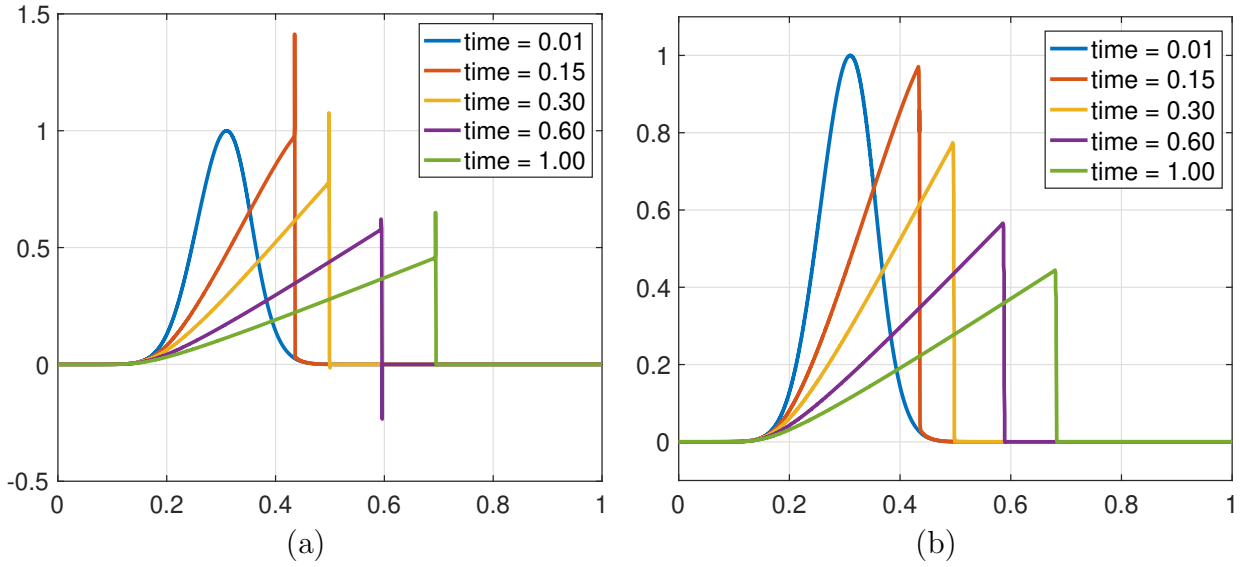

Figure 9: Example 6.5: Numerical solution of $h = \frac{1}{1000}$, $\Delta t = 10^{-4}$ and $k = 1$ for (a) scheme without limiter; (b) scheme with limiter.

Next, we perform the higher resolution simulation with and without WENO limiters and the numerical performance is illustrated in Figure 9. The WG linear solution on the mesh $h = 10^{-3}, \Delta t = 10^{-4}$ without limiter is plotted in Figure 9 (a). Oscillations are observed near discontinuities. In comparison, at each time step, we can perform the WENO limiter to filter out the oscillation and the numerical solutions are plotted in Figure 9 (b). As seen in this figure, the oscillation is removed and produced better numerical simulations for this Burgers equation.

6.6. Cauchy data as initial profile

In this example, we consider the initial profile as the Cauchy data

$$u(x,0) = \begin{cases} 2, & \text{if } x < 0 \\ 2 - x, & \text{if } 0 \le x \le 1 \\ 1, & \text{if } x > 1 \end{cases}. \tag{41}$$

The solution can be written as

$$u(x,t) = \begin{cases} 2, & \text{if } x < 2t \\ \dfrac{2-x}{1-t}, & \text{if } 2t \le x \le 1+t \\ 1, & \text{if } x > 1+t \end{cases}, \tag{42}$$

for $t \ge 0$.

The numerical solutions corresponding to the scheme without and with WENO limiter are plotted in Figure 10-11. Figure 10 (a) plots the simulation with $k = 1$ by solid lines for time = 0.1, 0.3, and 0.5. The exact solutions are illustrated as the dotted lines. Mild oscillations can be observed around $x = 2 \times$ time and $x = 1 +$ time. By employing the WENO limiter for each time

step, the numerical solution is plotted in Figure 10 (b). As removing the oscillations, we have improved the simulation. The similar conclusions can be made for the WG element with $k = 2$ in the Figure 11.

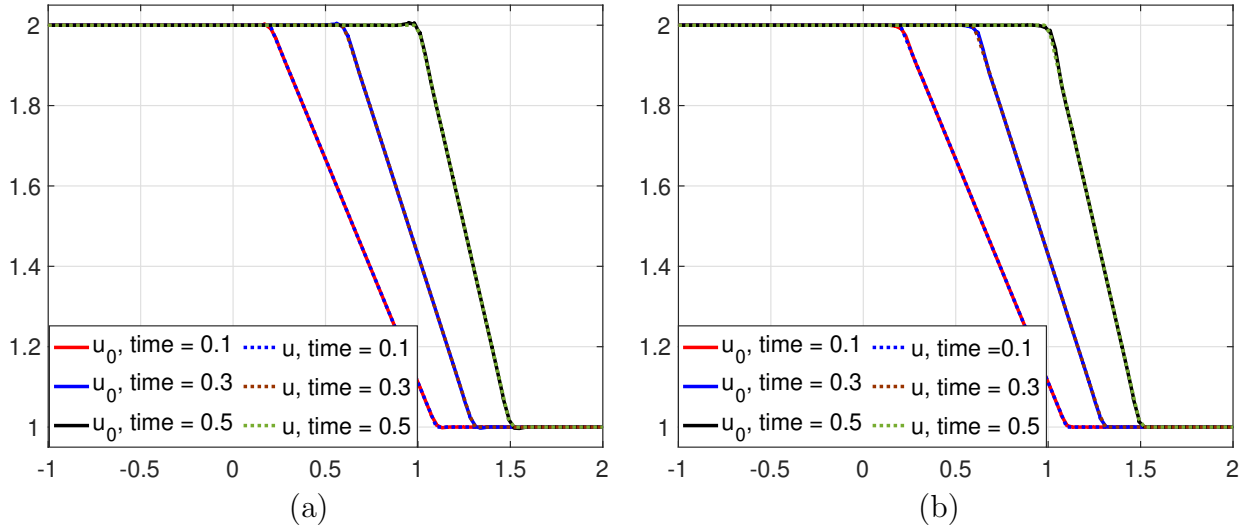

Figure 10: Example 6.6: WG solution on the mesh $h = 0.01$ with $k = 1$ for: (a) no limiter; (b) with WENO limiter.

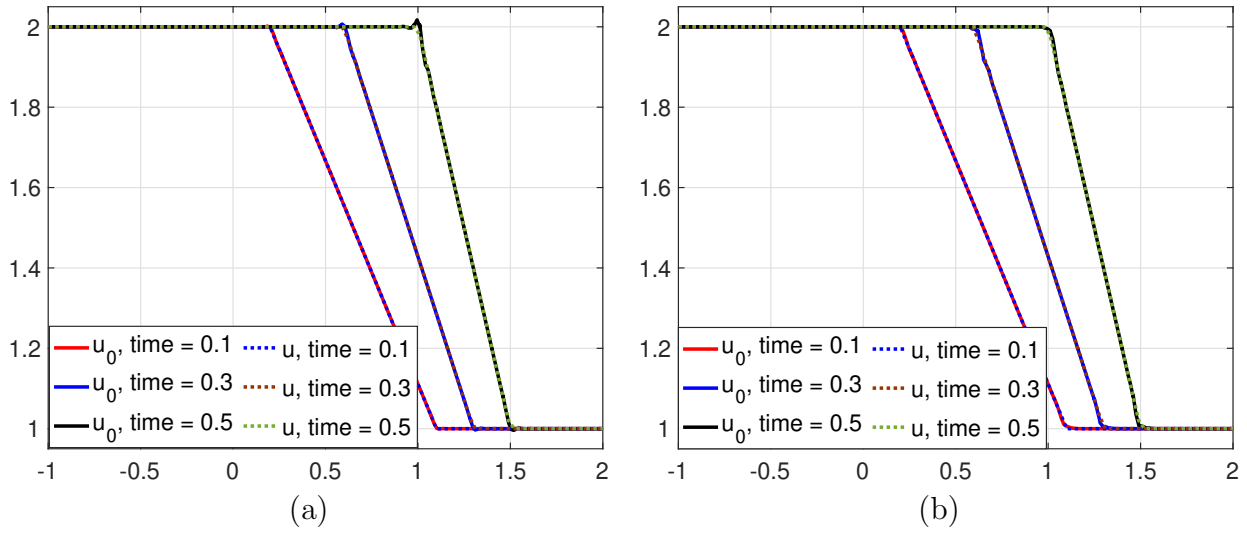

Figure 11: Example 6.6: WG solution on the mesh $h = 0.01$ with $k = 2$ for: (a) no limiter; (b) with WENO limiter.

6.7. Burgers' equation: discontinuous initial condition

We consider the Burgers' equation with homogeneous boundary conditions. The initial condition is taken to be a step function

$$u(0) = \begin{cases} 1, & \text{if } x \leq 0.5 \\ 0, & \text{if } x \geq 0.5 \end{cases}, \tag{43}$$

and choose the final time as $T = 0.60$.

For this problem, the wave speed is 0.5 and thus the exact solution is

$$u = \begin{cases} \dfrac{x}{t}, & \text{if } x < t, \\ 1, & \text{if } t \le x \le 0.5 + \dfrac{t}{2}, \\ 0, & \text{if } x > 0.5 + \dfrac{t}{2}. \end{cases}$$

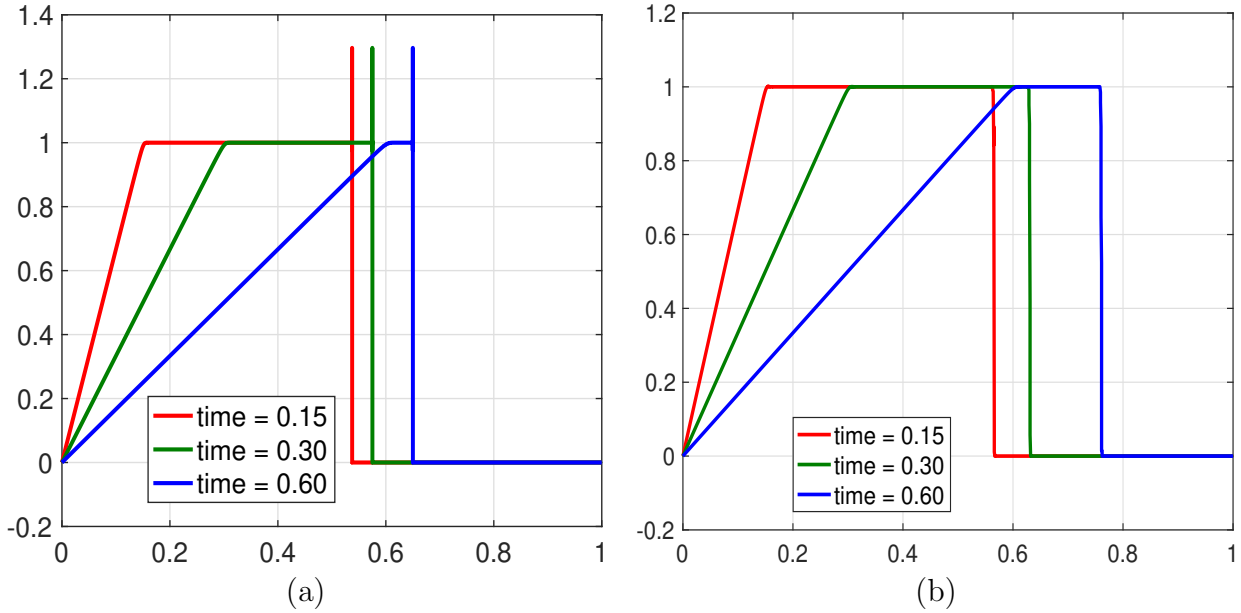

Figure 12: Example 6.7: Numerical solutions for linear WG scheme on mesh with $h = 10^{-3}$ and forward Euler scheme with $\Delta t = 10^{-4}$ for schemes (a) without limiter; (b) with limiter.

WG simulation with linear element is performed on the mesh with $h = 10^{-3}$, forward Euler method with $\Delta t = 10^{-3}$ for time stepping method and the numerical solution is plotted in Figure 12 (a). There are two issues related to this figure. First, the oscillations are shown near the shock front. Second, at time $= 0.6$, the shock front should be located at $x = 0.5 + \dfrac{0.6}{2} = 0.8$. However, the calculated shock front is slower than the real shock front.

The WENO limiter is employed for solving the first issue. We perform the limiter procedure at each time step for the same spatial and temporal discretization. The oscillations are removed by our limiter, which is shown in Figure 12 (b). However, the shock front is moving faster than the non-limiter one, but still slower than the exact shock front at time $= 0.6$, which should be at $x = 0.8$.

In order to improve the numerical performance, we conduct our scheme on forward Euler's method with $\Delta t = 10^{-5}$ and keep the simulation scheme (with WENO limiter) as previous experiment. The numerical solutions are compared with exact solutions in Figure 13(a). The numerical solutions and exact solutions are plotted by solid lines and dotted lines, respectively. One can

observe the well agreement in this figure. Besides, the mass values are illustrated in Figure 13 (b), which shows the mass conservation property.

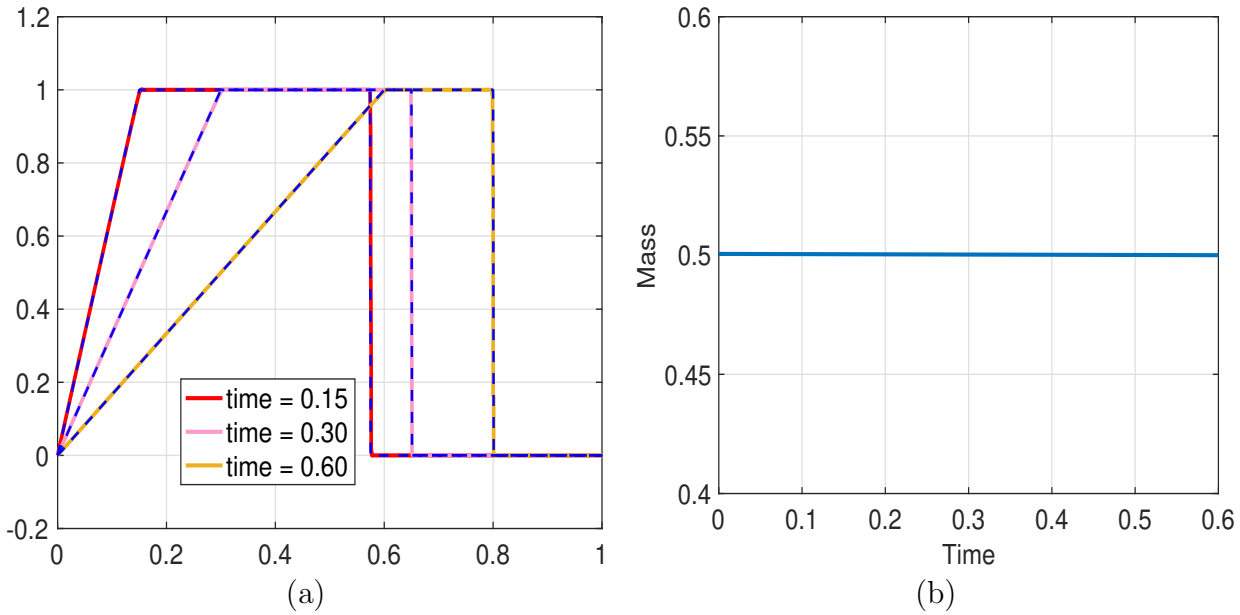

Figure 13: Example 6.7: (a) Numerical solutions for linear WG scheme on mesh with $h = 10^{-3}$ and forward Euler scheme with $\Delta t = 10^{-5}$ for schemes with limiter; (b) Plot of Mass value for the scheme in (a).

6.8. Rarefaction Wave

Let $I = [-1, 4]$, and consider the initial data as

$$u(x,0) = \begin{cases} 1, & x < 0 \\ 2, & x > 0 \end{cases}, \tag{44}$$

and the exact solution is a rarefaction wave of the form

$$u(x,0) = \begin{cases} 1, & x < t, \\ x/t, & t \le x \le 2t, \\ 2, & x > 2t. \end{cases} \tag{45}$$

We perform the linear WG simulation with WENO limiter on the mesh of $h = 10^{-3}$ and $\Delta t = 10^{-4}$ and the numerical solutions for various time are plotted in Figure 14. The numerical solutions are plotted with solid lines and the exact solutions are illustrated by dotted lines. Again, it shows that our approximation agrees with the exact solution very well.

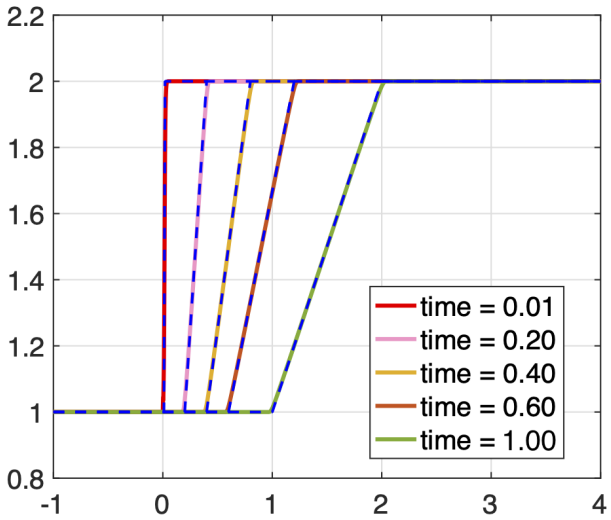

Figure 14: Example 6.8. Plot of numerical and exact solutions for different time. The numerical solutions are plotted by solid lines and the exact solutions are plotted by dotted lines.

7. Conclusion and Remark

In this paper, we have developed a new upwind weak Galerkin finite element method for time dependent hyperbolic equations. The upwind stabilizer has been utilized in the numerical scheme. Besides, in order to design the oscillation-free scheme, we have employed WENO limiter to reduce or remove the oscillation while remain the same mass quantity. The error estimate in L^2-norm has been provided and validated in the numerical tests. Then the same approach has been extended to Burgers equations.

As the future work plan, we shall extend the scheme to two dimensional and three dimensional Euler problems and Burgers problems. The associated stability and error analysis will be investigated in the future.

References

[1] V. Anaya, G. Gatica, D. Mora, and R. Ruiz-Baier, *An augmented velocity-vorticitypressure formulation for the Brinkman equations*, Internat. J. Numer. Methods Fluids, 79 (2015):109-137.

[2] R. Biswas, K. D. Devine and J. Flaherty, *Parallel, adaptive finite element methods for conservation laws*, Applied Numerical Mathematics, 14:255–283, 1994.

[3] F. Brezzi, B. Cockburn, L. Marini, E. Süli, *Stabilization mechanisms in discontinuous Galerkin finite element methods*, Comput. Methods Appl. Mech. Eng. 195 (2006): 3293–3310.

[4] A. Burbeau, P. Sagaut and Ch. H. Bruneau, *A problem-independent limiter for high order Runge-Kutta discontinuous Galerkin methods*, Journal of Computational Physics, 169:111–150, 2001.

[5] Y. Chen and T. Zhang, *A weak Galerkin finite element method for Burgers' equation*, Journal of Computational and Applied Mathematics 348 (2019): 103-119.

[6] B. Cockburn, S. Hou and C.-W. Shu, *The Runge-Kutta local projection discontinuous Galerkin finite element method for conservation laws IV: The multidimensional case*, Mathematics of Computation, 54:545–581, 1990.

[7] B. Cockburn, S.-Y. Lin and C.-W. Shu, *TVB Runge-Kutta local projection discontinuous Galerkin finite element method for conservation laws III: One-dimensional systems*, Journal of Computational Physics, 84:90–113, 1989.

[8] B. Cockburn and C.-W. Shu, *TVB Runge-Kutta local projection discontinuous Galerkin finite element method for conservation laws II: General framework*, Mathematics of Computation, 52:411–435, 1989.

[9] B. Cockburn and C.-W. Shu, *The Runge-Kutta local projection P1-discontinuous Galerkin method for scalar conservation laws*, Mathematical Modelling and Numerical Analysis, 25:337–361, 1991.

[10] B. Cockburn and C.-W. Shu, *The Runge-Kutta discontinuous Galerkin method for conservation laws V: Multidimensional systems*, Journal of Computational Physics, 141:199–224, 1998.

[11] B. Cockburn, and C. Shu, *Runge-Kutta discontinuous Galerkin methods for convection-dominated problems*, J. Sci. Comput. 16 (2001): 173–261.

[12] G. Fu, and C.-W. Shu, *A new troubled-cell indicator for discontinuous Galerkin methods for hyperbolic conservation laws*, Journal of Computational Physics, 347, 305-327, 2017.

[13] F. Gao, X. Wang, and L. Mu, *A modified weak Galerkin finite element methods for convection–diffusion problems in 2D*, Journal of Applied Mathematics and Computing, 49 (2015): 493-511.

[14] W. Guo, R. D. Nair, and X. Zhong, *An efficient WENO limiter for discontinuous Galerkin transport scheme on the cubed sphere*, Int. J. Numer. Meth. Fluids, 81: 3– 21, 2016.

[15] C. Johnson, and J. Pitkaranta, *An analysis of the discontinuous Galerkin method for a scalar hyperbolic equation*, Math. Comput. 46 (1986): 1–26.

[16] P. Lesaint, and P. Raviart, *On a finite element method for solving the neutron transport equation, Mathematical Aspects of Finite Elements in Partial Differential Equations*, Proc. Sympos., Math. Res. Center, Univ. Wisconsin, Madison, Wis., 1974.

[17] R. Lin, X. Ye, S. Zhang, and P. Zhu, *A Weak Galerkin Finite Element Method for Singularly Perturbed Convection-Diffusion-Reaction Problems*, SIAM Journal on Numerical Analysis, 56 (2018): 1482-1497.

[18] L. Mu, J. Wang, and X. Ye, *Weak Galerkin finite element methods for the biharmonic equation on polytopal meshes*, Numerical Methods for Partial Differential Equations, 30 (2014): 1003-1029.

[19] J. Qiu and C.W. Shu, *A comparison of troubled-cell indicators for Runge-Kutta discontinuous Galerkin methods using weighted essentially nonoscillatory limiters*, SIAM Journal on Scientific Computing, 27 (2005): 995–1013.

[20] D. Ray, and J. S. Hesthaven, , An artificial neural network as a troubled-cell indicator. Journal of computational physics, 367, 166-191, 2018.

[21] D. Ray, and J. S. Hesthaven, *Detecting troubled-cells on two-dimensional unstructured grids using a neural network*, Journal of Computational Physics, 397, 108845, 2019.

[22] W. Reed, and T. Hill, *Triangular mesh methods for the neutron transport equation, Tech*, Report LA- UR-73-479, Los Alamos Scientific Laboratory (1973).

[23] A. AL-Taweel, L. Mu, *A New Upwind Weak Galerkin Finite Element Method for Linear Hyperbolic Equations*, Preprint.

[24] M. J. Vuik, J. K. Ryan, *Multiwavelet troubled-cell indicator for discontinuity detection of discontinuous Galerkin schemes*, Journal of Computational Physics, 270, 138-160, 2014.

[25] J. Wang, and X. Ye, *A weak Galerkin finite element method for second-order elliptic problems*, Journal of Computational and Applied Mathematics, 241 (2013): 103-115.

[26] J. Wang, and X. Ye, *A weak Galerkin finite element method for the Stokes equations*, Advances in Computational Mathematics, 42 (2016): 155-174.

[27] R. Wang, X. Wang, Q. Zhai, and R. Zhang, *A weak Galerkin finite element scheme for solving the stationary Stokes equations*, Journal of Computational and Applied Mathematics, 302 (2016): 171-185.

[28] X. Zheng, and X. Xie, *A posteriori error estimator for a weak Galerkin finite element solution of the Stokes problem*, East Asian Journal on Applied Mathematics, 7 (2017): 508-529.

[29] J. Zhu, X.Zhong, C.-W. Shu, and J. Qiu, *Runge–Kutta discontinuous Galerkin method using a new type of WENO limiters on unstructured meshes*, Journal of Computational Physics, 248, 200-220, 2013.

[30] J. Zhu, X.Zhong, C.-W. Shu, and J. Qiu, *Runge-Kutta discontinuous Galerkin method with a simple and compact Hermite WENO limiter*, Communications in Computational Physics 19(4): 944-969, 2016.

[31] J. Zhu, X.Zhong, C.-W. Shu, and J. Qiu, *Runge-Kutta Discontinuous Galerkin Method with a Simple and Compact Hermite WENO Limiter on Unstructured Meshes*, Communications in Computational Physics, 21(3), 623-649, 2017.

[32] X. Zhong and C.W. Shu, *A simple weighted essentially nonoscillatory limiter for Runge–Kutta discontinuous Galerkin methods*, Journal of Computational Physics, 232 (2013): 397-415.